catalysts

MDPI

Article

Carbon Dioxide Valorization into Methane Using Samarium Oxide-Supported Monometallic and Bimetallic Catalysts

Radwa A. El-Salamony [1], Ahmed S. Al-Fatesh [2,*], Kenit Acharya [3], Abdulaziz A. M. Abahussain [2], Abdulaziz Bagabas [4], Nadavala Siva Kumar [2], Ahmed A. Ibrahim [2], Wasim Ullah Khan [5] and Rawesh Kumar [3,*]

1 Process Development Department, Egyptian Petroleum Research Institute (EPRI), Cairo 11727, Egypt
2 Chemical Engineering Department, College of Engineering, King Saud University, P.O. Box 800, Riyadh 11421, Saudi Arabia
3 Department of Chemistry, Indus University, Ahmedabad 382115, Gujarat, India
4 President Office, King Abdulaziz City for Science and Technology (KACST), P.O. Box 6086, Riyadh 11442, Saudi Arabia
5 Chemical and Process Engineering, College of Engineering, University of Canterbury, Christchurch 8041, New Zealand
* Correspondence: aalfatesh@ksu.edu.sa (A.S.A.-F.); kr.rawesh@gmail.com (R.K.)

Abstract: Samarium oxide (Sm_2O_3) is a versatile surface for CO_2 and H_2 interaction and conversion. Samarium oxide-supported Ni, samarium oxide-supported Co-Ni, and samarium oxide-supported Ru-Ni catalysts were tested for CO_2 methanation and were characterized by X-ray diffraction, nitrogen physisorption, infrared spectroscopy, H_2-temperature programmed reduction, and X-ray photoelectron spectroscopy. Limited H_2 dissociation and widely available surface carbonate and formate species over 20 wt.% Ni, dispersed over Sm_2O_3, resulted in ~98% CH_4 selectivity. The low selectivity for CO could be due to the reforming reaction between CH_4 (methanation product) and CO_2. Co-impregnation of cobalt with nickel over Sm_2O_3 had high surface adsorbed oxygen and higher CO selectivity. On the other hand, co-impregnation of ruthenium and nickel over Sm_2O_3 led to more than one catalytic active site, carbonate species, lack of formate species, and 94% CH_4 selectivity. It indicated the following route of CH_4 synthesis over Ru-Ni/Sm_2O_3; carbonate → unstable formate → CO → CH_4.

Keywords: CO_2 methanation; CH_4 selectivity; Sm_2O_3-supported Ni; Sm_2O_3-supported Co-Ni; Sm_2O_3-supported Ru-Ni

check for updates

Citation: El-Salamony, R.A.; Al-Fatesh, A.S.; Acharya, K.; Abahussain, A.A.M.; Bagabas, A.; Kumar, N.S.; Ibrahim, A.A.; Khan, W.U.; Kumar, R. Carbon Dioxide Valorization into Methane Using Samarium Oxide-Supported Monometallic and Bimetallic Catalysts. *Catalysts* **2023**, *13*, 113. https://doi.org/10.3390/catal13010113

Academic Editor: Gilles Berhault

Received: 6 November 2022
Revised: 21 December 2022
Accepted: 28 December 2022
Published: 4 January 2023

Copyright: © 2023 by the authors. Licensee MDPI, Basel, Switzerland. This article is an open access article distributed under the terms and conditions of the Creative Commons Attribution (CC BY) license (https://creativecommons.org/licenses/by/4.0/).

1. Introduction

The global concentration of carbon dioxide (CO_2) has already reached dangerous levels, where island countries and temperature-sensitive animals are on the borderline of extinction due to global warming. It has affected the seasonal cycles and has brought natural disasters across the globe. If the scientific community did not find a way of decreasing CO_2 concentration in the nearby future, the worst days would be faced. Besides the strategy of reducing CO_2 emissions, scientific findings for the conversion of CO_2 into useful chemicals are also encouraged worldwide [1,2].

The catalytic conversion of CO_2 over metal oxide, doped metal oxide, and supported metal oxide has received the highest attention due to its catalytic potential, heterogeneity, and high-temperature sustainability. CO_2 and H_2 interaction over catalytic surface generates variety of products from hydrocarbon (olefin and paraffin) to oxygenates (CH_3OH, CH_3COOH) [3–7]. Formate is a surface-bonded carbon dioxide species, whereas hydrogen is easily dissociated over a metal surface such as iron, copper, silver, gold, platinum, palladium, rhodium, molybdenum, rhenium, or nickel [6,8–10]. Controlling catalytic surfaces

becomes crucial to understanding product distribution. Formate species is not stable, except over Ni, and it is decomposed into CO under H_2 flow through reverse water–gas shift reaction. Copper oxide (CuO) showed just 13% CO_2 conversion with 10.4% CO yield and iron (III) oxide (Fe_2O_3) showed 8% CO_2 conversion with 6.3% CO yield [11], indicating that unsupported CuO and Fe_2O_3 were not effective catalysts. Thus, the concept of promoted and supported metal catalysts has come into the picture, where the catalytic efficiency is augmented in terms of the dispersion of catalytic active sites over proper support and the role of promoters in modifying the physiochemical properties of supported catalyst systems. The comprehensive reaction scheme over the supported metal catalyst is shown in Figure 1.

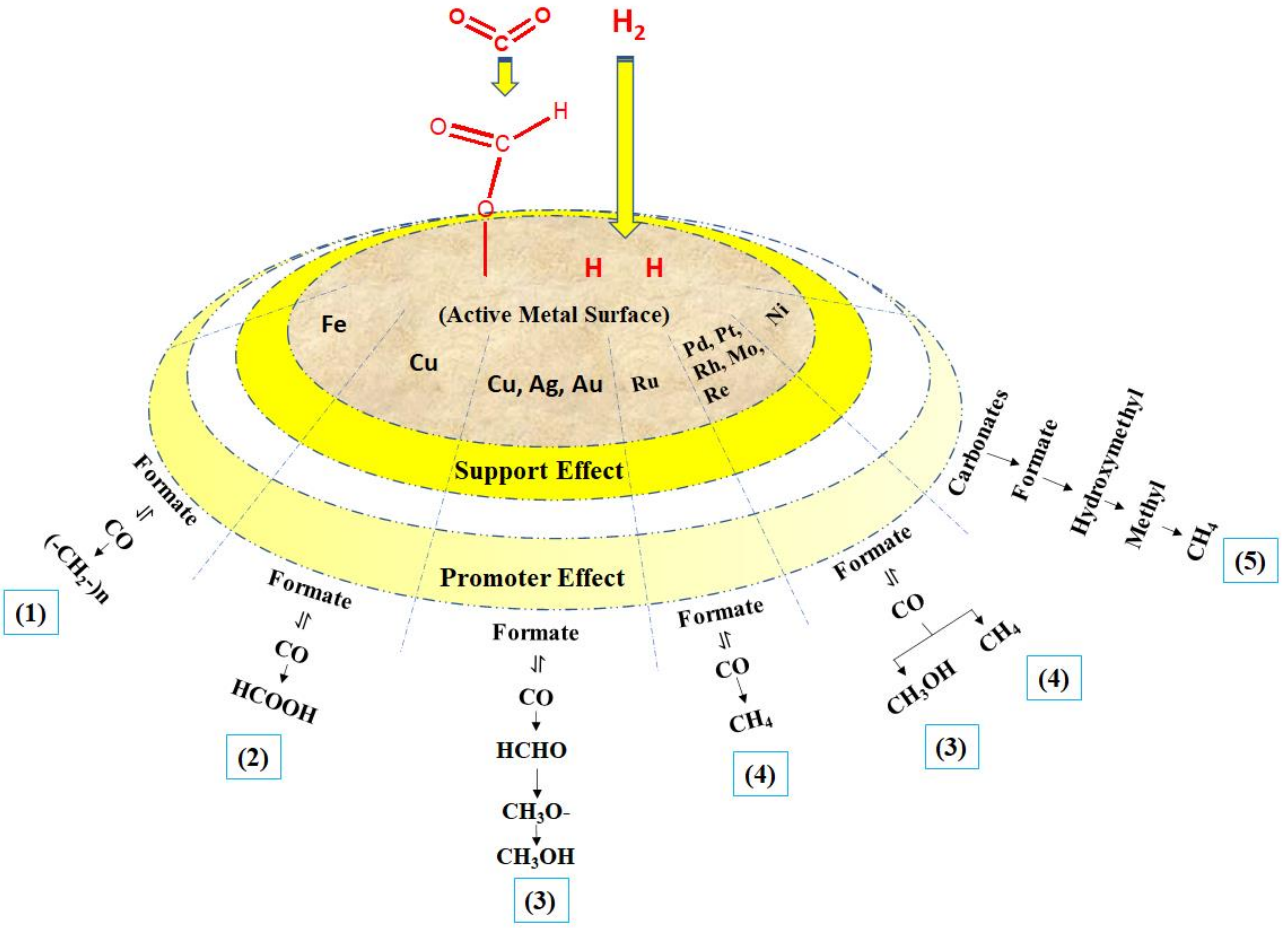


Figure 1. Reaction scheme of CO_2 and H_2 interaction over supported metal catalyst.

When a "supported active metal iron" catalyst is utilized, carbon monoxide is converted into metal carbide, switches to the chain growth mechanism, and gives C1 to higher hydrocarbon (concerned with olefin and paraffin; Route 1) [12]. For route 1, the potassium- and copper-promoted, Al_2O_3-supported iron (Fe-Cu-K-Al) catalyst has been studied extensively [8,13,14]. Over the Cu-supported catalyst, CO hydrogenation takes place in two ways: the formic acid route (Route 2) and the methanol route through formaldehyde and methoxide intermediate (Route 3) [15]. The zirconium-promoted CuO-ZnO-Al_2O_3 (1:1:1) catalyst has received wide attention for high CO_2 conversion and high CH_3OH selectivity [9]. The supported Ag and Au catalysts prefer route 3 [10]. Supported 5.0 wt.% Ru metal induces an eight electron reduction in intermediate CO into CH_4 (Route 4) [6]. The Al_2O_3-supported Ru catalyst had an atomic assembly with high dispersion of three dimensional Ru cluster. It showed about 55% CO_2 conversion with 55% CH_4 yield. Pd, Pt, Rh, Mo, and Re metals direct CO_2 and H_2 through routes 3 and 4, which lead to high

selectivity to methanol and methane, respectively [10]. On the other hand, the supported Ni catalyst carries CO_2 in the CO_x-free catalytic route (CO_2 methanation route): $CO_2 \rightarrow$ carbonate $\rightarrow$ formate $\rightarrow$ $-CH_2OH \rightarrow -CH_3 \rightarrow CH_4$ (Route 5) [16]. This route is useful in generating CO_x-free CH_4. Incorporating Co in Ni led to a smaller lattice constant and higher hydrogenation activity of CO_2 [17,18]. Cobalt-based catalysts were also investigated greatly for CO_2 conversion into light hydrocarbons [19].

Al_2O_3-supported Ni catalysts showed 50% CO_2 conversion with 50% CH_4 yield [20], while 3.0 wt.% Zr-promotional addition inhibited migration of Ni into Al_2O_3 matrix or inhibited the formation of $NiAl_2O_4$, caused >60% CO_2 conversion and 70% CH_4 yield [21]. The activity of La_2O_3-supported Ni catalyst toward CO_2 methanation was worse because of the formation of stable lanthanum carbonate [$La_2(CO_3)_3$], which did not decompose into formate [20]. In addition, the SiO_2-supported Ni catalyst was not good for CO_2 methanation because of the collapse of the Si-O-Si structure by hydrolysis of water, sintering of Ni particles, and rapid coke deposition and deactivation of the catalyst [22]. Among supported catalyst systems, the Y_2O_3-supported Ni catalyst displayed the maximum CO_2 conversion (75%) with 75% CH_4 yield due to the presence of more basic sites and easily reducible NiO species. However, in terms of CH_4 selectivity, the ZrO_2-supported Ni catalyst resulted in the best (60% CO_2 conversion with 100% CH_4 selectivity) [23].

For such an important reaction, other supports should also be investigated continuously. For instance, Sm_2O_3 had various favorable surface properties for CO_2 and H_2 interaction. It had Ni-size optimizing capacity like Y_2O_3, higher Ni dispersion and a stronger metal-support interaction than Y_2O_3 [24,25]. Electrochemically reduced Sm(II) compound was found to be a powerful catalyst for CO_2 activation [26]. Sm_2O_3 was utilized in quantitative detection of CO_2 and CO [27]. Moreover, a 5 atom% Sm addition over the Ni-Zr catalyst induced a higher H_2 uptake [28]. Muroyama et al. showed that upon reduction, the Ni particle size distribution was the narrowest and their sizes were the smallest over Sm_2O_3 compared to other supports (Y_2O_3, Al_2O_3, La_2O_3, and ZrO_2) [20]. A 5.0 wt.% Ni loading over Sm_2O_3 achieved 100% CH_4 selectivity, but with ~20% CO_2 conversion at 300 °C [29]. Upon incorporation of a 5.0 wt.% Ba into the Sm_2O_3-supported Ni catalyst, the CH_4 selectivity remained 100% and CO_2 conversion was maintained at 40% for 28-h TOS at 300 °C. The CO-free, high-performance catalytic route of the 5 wt.%Ni-5 wt.%Ba/Sm_2O_3 catalyst was due to the enhanced oxygen mobility (causing more oxygen vacancy), increased CO_2 adsorption (causing the formation of more surface carbonate species), and enhanced hydrogenation of carbonate into formate species.

Inspired by its properties in favor of CO_2 and H_2 interaction, samarium oxide-supported Ni, samarium oxide-supported Co-Ni, and samarium oxide-supported Ru-Ni catalysts were prepared by the impregnation and co-impregnation method and were tested for CO_2 methanation. Catalysts were characterized by X-ray diffraction (XRD), surface area and porosity, infrared spectroscopy, H_2-temperature programmed reduction (H_2-TPR), and X-ray photoelectron spectroscopy (XPS). Fine-tuning between surface properties and characterization results was found. This thorough study would help to understand the surface behavior of Sm_2O_3-supported metal catalysts toward CO_2 methanation reaction.

2. Results

2.1. Characterization Results

Energy Dispersive X-ray (EDX) elemental analysis of 10Ni/Sm_2O_3, 20Ni/Sm_2O_3, 40Ni/Sm_2O_3, 10Ni-10Co/Sm_2O_3 and 10Ni-10Ru/Sm_2O_3 catalysts is shown in Figure S1. EDX elemental analysis showed that with increasing 10 wt.% to 40 wt.% Ni loading, surface atomic composition of Ni was increasing. The 10Ni-10Co/Sm_2O_3 catalyst showed that the surface composition of Ni over the 10Ni-10Co/Sm_2O_3 catalyst was minimum, whereas surface composition of Ni was maximum at 10Ni-10Ru/Sm_2O_3 catalyst. The X-ray diffraction results of the catalyst samples are shown in Figure 2 and diffraction peaks are matched with Joint Committee on Powder Diffraction Standards (JCPDS) reference card number. All catalysts showed low intensity diffraction peaks. The support had diffraction

peaks for the Sm_2O_3 phases at 2θ = 27.68°, 28.11°, 29.04°, 29.74°, 30.64°, 31.09°, 31.86°, 32.61°, 38.59°, 40.51°, 46.73°, 50.13°, 51.44°, 53.24°, 54.70°, 55.72° (JCPDS reference card number 00-013-0244 and 00-042-1461). Upon the 10.0 wt.% Ni addition, the intensity for the diffraction peaks for the Sm_2O_3 phases decreased significantly. However, the peaks of the cubic NiO phase were not detected, indicating that up to 10 wt.% Ni loading over the Sm_2O_3, NiO was well-dispersed (Figure 2A). NiO dispersion and the reduction in the peak intensity of Sm_2O_3 in the $10Ni/Sm_2O_3$ catalyst suggested the close interaction of NiO with Sm_2O_3 support. The same type of finding was observed over the Y_2O_3-supported Ni catalyst [30]. Upon increasing the NiO loading to 20.0 wt.%, the cubic NiO phase appeared at 2θ = 37.24°, 43.28°, 62.75° (JCPDS reference card number 01-073-1523) (Figure 2B). Furthermore, increasing the NiO loading to 40 wt.% led only to the observation of the diffraction peaks of Sm_2O_3 without detecting those diffraction peaks of the cubic NiO phase (Figure 2C). The diffraction patterns of $40Ni/Sm_2O_3$ and $10Ni/Sm_2O_3$ were comparable. However, the bimetallic catalyst of 10 wt.%Co-10 wt.%Ni, dispersed over Sm_2O_3 support, had a very similar diffraction pattern to that of $20Ni/Sm_2O_3$ (Figure 2D). It indicated that in presence of CoO, the NiO crystalline phase was relatively more exposed (like $20Ni/Sm_2O_3$). The bimetallic catalyst of 10 wt.%Ru-10 wt.%Ni, dispersed over Sm_2O_3 support, had no crystalline peaks for NiO, but it had diffraction peaks for the Sm_2O_3 phase and for the tetragonal RuO_2 phase (at 2θ = 35.02°; JCPDS reference card number 00-040-1290) (Figure 2E).

The N_2-adsorption isotherms, porosity distribution, BET surface area, BJH pore volume, and BJH pore diameter are depicted in Figure 3A,B and Figure S2. All samples showed type-IV isotherm with H3 hysteresis loop, which indicated non-rigid aggregates like-pore with unlimited adsorption at high p/p^0 [31]. The Sm_2O_3-supported 10 wt.% Ni catalyst had the least surface area, and pore volume among the remaining supported catalysts. However, upon 20.0 wt.% Ni loading, the height of the hysteresis loop was amplified and the surface area, pore volume, and pore diameter were increased to four times (25.70l m^2/g), six times (0.175 cc/g) and seven times (15.797 nm), respectively, implying that Ni did not only disperse over the catalyst surface, but also it was incorporated into the Sm_2O_3 framework and caused expansion of framework [29]. Upon 40.0 wt.% Ni impregnation, the height of the hysteresis loop was decreased sharply, and the surface area and pore volume were decreased sharply (to 12.7 m^2/g and 0.061 cc/g, respectively) without affecting the pore diameter. It indicated the pore blocking by inclusions of NiO nanoparticles [32] upon higher loading. Co-impregnation of 10.0 wt.% Co and 10.0 wt.% Ni over Sm_2O_3 support was found to maximize the surface area and pore volume up to the highest limit (with respect to the rest catalysts). The surface area and pore volume of $Co\text{-}Ni/Sm_2O_3$ were enhanced more than 10 times without affecting the pore diameter (with respect to $10Ni/Sm_2O_3$). The height of the hysteresis loop in the isotherm plot of the $Co\text{-}Ni/Sm_2O_3$ catalyst was also enhanced up to the highest extent. However, with a co-impregnation of 10.0 wt.% Ru and 10.0 wt.% Ni over Sm_2O_3 support, the surface parameters were dropped. In XRD, the tetragonal RuO_2 was detected over the $Ru\text{-}Ni/Sm_2O_3$ catalyst, indicating that a sharp drop of the surface parameters was due to the large deposition of tetragonal RuO_2 crystals into the pore of the catalyst. These phenomena are related mainly to the ionic radii of the employed metals, where in the case of Co ions, the ionic radius was equal to that of Ni ions, but in the case of Ru, it was bigger. These findings are coincident with our previous study on Y_2O_3 support [33]. It appeared that in the case of co-impregnation, the pore diameter of the catalyst was not modified and the pore diameter of $Co\text{-}Ni/Sm_2O_3$ and $Ru\text{-}Ni/Sm_2O_3$ and $10Ni/Sm_2O_s$ were within the range from 2.0 to 2.4 nm. These observations were quite informative and indicated the uptake capacity of the heteroatom in the Sm_2O_3 framework. If 10 wt.% Ni loading was taken as a standard, then further 10 wt.% loading of Ni on Sm_2O_3 caused the expansion of the entire framework. However, when 10 wt.% Co along with 10 wt.% Ni (total 10 wt.%Co-10 wt.% Ni) was loaded over Sm_2O_3, Co was incorporated in the Sm_2O_3 framework except on the pore opening of the surface. Thus, pore volume and surface area were increased, but not the pore size. During loading of 10 wt.% Ru along

with 10 wt.% Ni over Sm_2O_3, RuO_2 particles were largely deposited in the pore, causing decrements in all surface parameters.

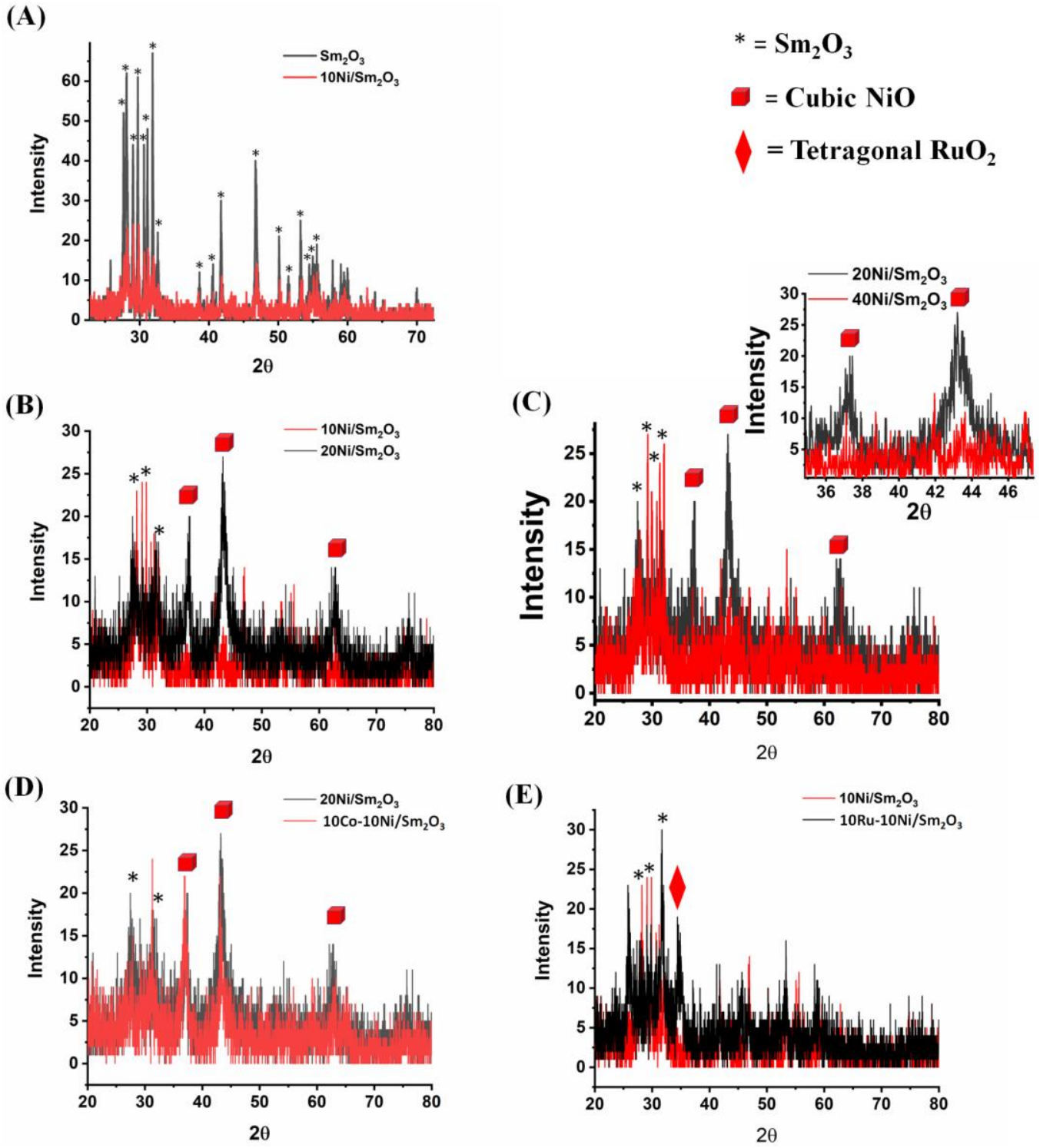
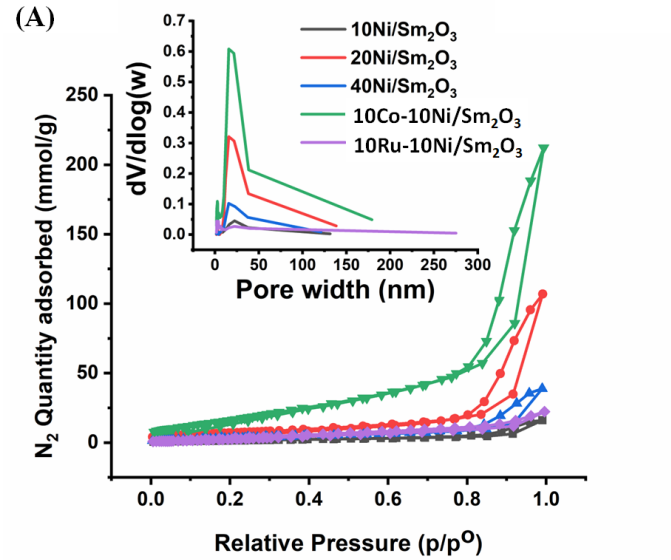
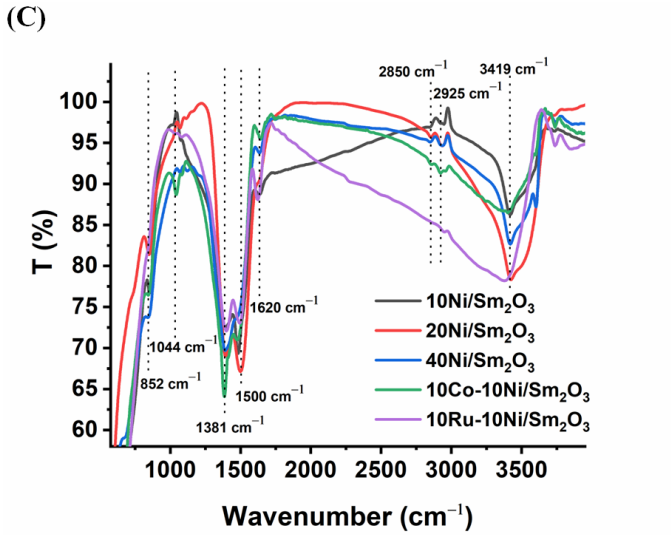


Figure 2. X-ray diffraction profiles of (**A**) Sm_2O_3 and $10Ni/Sm_2O_3$ (**B**) $10Ni/Sm_2O_3$ and $20Ni/Sm_2O_3$ (**C**) $20Ni/Sm_2O_3$ and $40Ni/Sm_2O_3$ (**D**) $20Ni/Sm_2O_3$ and $10Co\text{-}10Ni/Sm_2O_3$ (**E**) $10Ni/Sm_2O_3$ and $10Ru\text{-}10Ni/Sm_2O_3$.



(B)

Catalyst Sample	Surface Area (m^2/g)	Pore Volume (cc/g)	Pore Diameter (nm)
$10Ni/Sm_2O_3$	6.105	0.026	2.194
$20Ni/Sm_2O_3$	25.701	0.175	15.797
$40Ni/Sm_2O_3$	12.689	0.061	15.709
$10Co\text{-}10Ni/Sm_2O_3$	69.589	0.357	2.390
$10Ru\text{-}10Ni/Sm_2O_3$	13.327	0.040	2.028



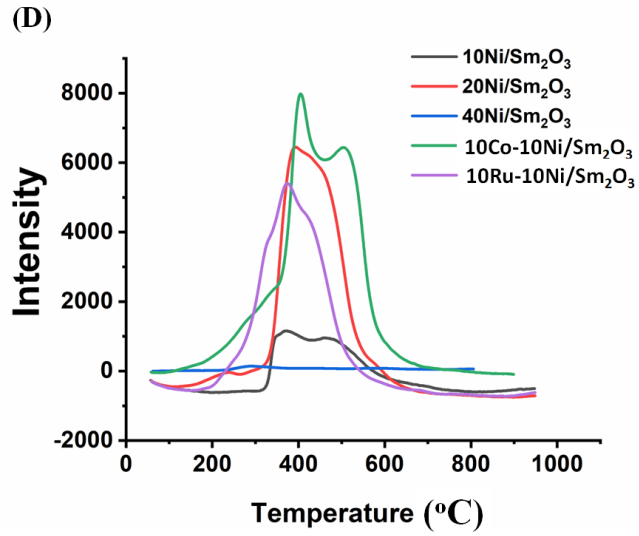


Figure 3. (**A**) N_2 adsorption isotherms of the prepared catalysts (**B**) Table indicating the surface area, pore volume, and pore diameter of the different catalysts (**C**) Infrared transmittance spectra of the different catalysts (**D**) H_2-temperature programmed reduction profiles of the different catalysts.

Infrared (IR) spectra of the catalyst samples are shown in Figures 3C and S3. The IR band at ~1620 cm^{-1} and 3429 cm^{-1} could be attributed to the bending and stretching vibrations of the hydroxyl groups over the catalyst surface, respectively [34]. These two bands were present even in the bare support of Sm_2O_3 (Figure S3). Upon Ni loading over Sm_2O_3, various other prominent bands appeared. The transmittance peak was at 852 cm^{-1} for CO_3^{2-} symmetric stretching, 1044 cm^{-1} for the vibration of bidentate carbonate species, 1381 cm^{-1} and 1500 cm^{-1} for the vibration of unidentate carbonate species [35–37], 2850 cm^{-1} for the stretching vibration of C-H (of coordinated formate species), and 2925 cm^{-1} for the combination of the asymmetric stretching of –COO and the bending vibration of C–H bond (of bi-coordinated formate species) [38]. Interaction of CO_2 with samarium (through different CO_2 intermediates) was previously reported [39]. The IR spectra of the $20Ni/Sm_2O_3$ catalyst could be specified by the intense spectral vibration of the unidentate carbonate species at 1500 cm^{-1}, whereas the $Co\text{-}Ni/Sm_2O_3$ catalyst had the most intense vibration for the bicarbonate species at 1044 cm^{-1}, and the unidentate carbonate species at 1381 cm^{-1}. It is noticeable that the $Ru\text{-}Ni/Sm_2O_3$ catalyst had no vibration bands for the formate species (~2850 cm^{-1} and 2925 cm^{-1}).

The Sm_2O_3-supported 10 wt.% Ni catalyst had reduction peaks at 360 °C and 475 °C with total adsorption of 2.197 mmol/g of H_2. The earlier one was attributed to the reduction in NiO species, which interacted weakly with support, while the latter peak was attributed to the reduction in NiO species, which interacted strongly with the support [40]. For higher Ni loading (20.0 wt.%), the $20Ni/Sm_2O_3$ catalyst had the highest H_2 consumption (7.28 mmol/g) among the other Ni-loaded Sm_2O_3 catalysts with a merge reduction peak in the temperature range 327–615 °C (the peak maximum ~400 °C). It indicated the presence of a high concentration of reducible NiO species, interacting with the support up to different extents. For 40.0 wt.% Ni loading, the $40Ni/Sm_2O_3$ catalyst had the worst reducible profile. It had a negligible amount of reducible NiO species (0.244 mmol/g H_2 consumption). Accordingly, $40Ni/Sm_2O_3$ had minimum reducibility. The reducibility profile of the bimetallic Co-Ni, dispersed over Sm_2O_3, had the maximum amount of H_2 consumption (8.827 mmol/g) among all catalysts. The $Co-Ni/Sm_2O_3$ catalyst had the highest intensity of reducible peak about the peak maxima at 400 °C for the reduction in NiO-interacted species, low-temperature overlapping peaks ~300 °C for the reduction in Co_3O_4 to CoO, and a high-temperature reduction peak ~500 °C for the reduction in CoO to Co [41,42]. However, the high-temperature reduction peak ~500 °C in the $Co-Ni/Sm_2O_3$ catalyst might be related to the combining contributions of reducible NiO and CoO species. The H_2-consumption profile of the bimetallic Ru-Ni, dispersed over Sm_2O_3, showed an additional reduction peak at a relatively lower temperature (~330 °C) for a partial reduction in dispersed RuO_x species on the support [43]. The total hydrogen consumption of the $Ru-Ni/Sm_2O_3$ catalyst in the H_2-temperature programmed reduction study was found 6.25 mmol/g.

There is a marked difference in the surface characteristics of both supported bimetallic catalysts. To understand the valance state and bonding character: Ni (2p), Sm (3d) and O (1s) XPS spectra of the $Co-Ni/Sm_2O_3$ and $Ru-Ni/Sm_2O_3$ catalysts were depicted in Figure 4A–D. The Ni2p spectra of both Sm_2O_3-supported bimetallic catalysts had mostly similar profiles. The absence of metallic Ni peak (about binding energy <854 eV and 869–870 eV) in Ni2p XPS spectra was confirmed in the $Co-Ni/Sm_2O_3$ and $Ru-Ni/Sm_2O_3$ catalysts [44,45]. The presence of Ni^{+2} oxidation state in the form of NiO compound was confirmed by $Ni2p_{1/2}$ spectra ~871.8–873.8 eV and 879 eV, and $Ni2p_{3/2}$ spectra ~854.3–855.7 eV [46–49] (Figure 4A). $Sm3d_{3/2}$ and $Sm3d_{5/2}$ spectra at ~1110.25 eV and 1083.24 eV, respectively, indicated the presence of Sm^{+3} oxidation state (Sm_2O_3 compound) [50,51] (Figure 4C). The binding energy values of the O1s profiles indicated the overlapping contributions of oxygen from various oxide species [52]. The O1s spectra with binding energy at 531.2 eV and 530 eV were noticed in both the $Co-Ni/Sm_2O_3$ and $Ru-Ni/Sm_2O_3$ catalysts (Figure 4D). The binding energy at 531.2 eV was attributed to adsorbed oxygen [53], whereas the binding energy at 530 eV signified the oxygen in samarium oxide [51]. Both XPS peak intensities were much less in the $Ru-Ni/Sm_2O_3$ catalyst than to their corresponding ones in the $Co-Ni/Sm_2O_3$ catalyst, indicating the availability of "surface adsorbed oxygen" and oxygen in samarium oxide in the $Co-Ni/Sm_2O_3$ catalyst. To bring more focus on the valance state and bonding character of the second metal over the Sm_2O_3-supported Ni catalyst, the Co (2p) spectrum of the $Co-Ni/Sm_2O_3$ catalyst and the Ru (3d) spectrum of the $Ru-Ni/Sm_2O_3$ catalyst were also recorded, as depicted in Figure S4, respectively. Co2p XPS spectra did not show a peak for metallic Co at binding energy ~778 eV, but it showed a peak with a binding energy centered at 780 eV for $2p_{3/2}$) for Co_3O_4 [42]. The Ru3d spectrum of the $Ru-Ni/Sm_2O_3$ catalyst showed a broad overlapping peak in the binding energy range 281.5–285 eV. It indicated the presence of Ru oxide species [54,55].

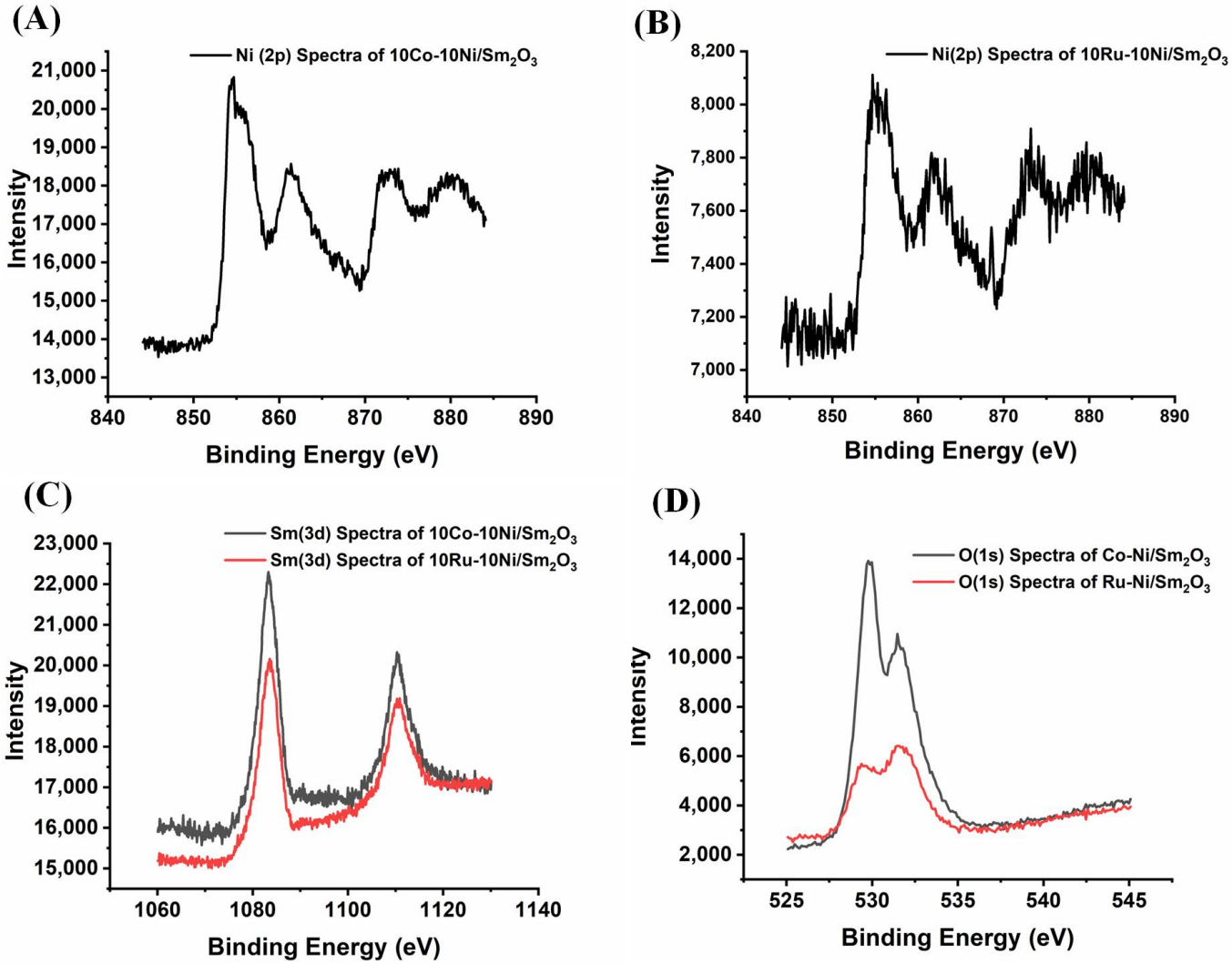


Figure 4. (**A**) Ni (2p) core-level XPS spectrum of Co-Ni/Sm_2O_3 (**B**) Ni (2p) core-level XPS spectrum of Ru-Ni/Sm_2O_3 catalyst (**C**) Sm (3d) XPS spectra of Co-Ni/Sm_2O_3 and Ru-Ni/Sm_2O_3 catalyst (**D**) O (1s) core-level XPS spectra of Co-Ni/Sm_2O_3 and Ru-Ni/Sm_2O_3 catalyst.

2.2. Catalytic Activity Result and Discussion

The reaction temperature suitable for CO_2 methanation was tested over the 10Ni/Sm_2O_3 catalyst and was depicted in Figure S5. It was found that the mole% of CH_4 formation from CO_2 and H_2 was negligible at 250 °C, notable at 300 °C, and prominent at 350 °C. At 350 °C temperature, the mole% of CO formation was null, which indicated that CH_4 formation was carried out without including CO in the intermediate reaction step. In infrared spectra, a peak for formate was observed in all catalysts except 10Ru-10Ni/Sm_2O_3. The literature report suggested stable formate formation over the Ni-based catalyst system, which further underwent successive hydrogenation to methane through the methoxy intermediate route [16]. Thus, 350 °C was kept standard for CO_2 methanation over our the Sm_2O_3-supported Ni catalyst system. Other research groups also found 350 °C as the suitable temperature for CO_2 methanation [56–58]. The catalytic activity of the xNi/Sm_2O_3 (x = 10, 20, 40) and M-Ni/Sm_2O_3 (M = Co, Ru) catalysts in the term of CO_2 conversion, CH_4 selectivity, and CO selectivity are shown in Figure 5. XRD did not detect metallic Ni or NiO phase over the Sm_2O_3-supported 10.0 wt.% Ni catalyst and H_2-TPR indicated the reduction peaks of NiO-interacted species. IR confirmed the presence of surface interacted CO_2-species such carbonate and formate over 10Ni/Sm_2O_3 surface. Overall, 10Ni/Sm_2O_3 had widely available surface-interacted CO_2-species and reducible NiO species (inducing

H_2 dissociation and spillover). The CO_2 conversion remained constant at ~35% for 13 h, but constant selectivities for CO and CH_4 were attained after 100 min of reaction. Initially, the CO and CH_4 selectivities were comparative (47% and 52%), but after 100 min, the CO selectivity dropped to 5–6%, whereas the CH_4 selectivity jumped to 94–95%. Further, the constant CH_4 and CO selectivities were maintained for 13 h time-on-stream. This finding indicated that the $10Ni/Sm_2O_3$ catalyst system needed some time for constant product selectivity.

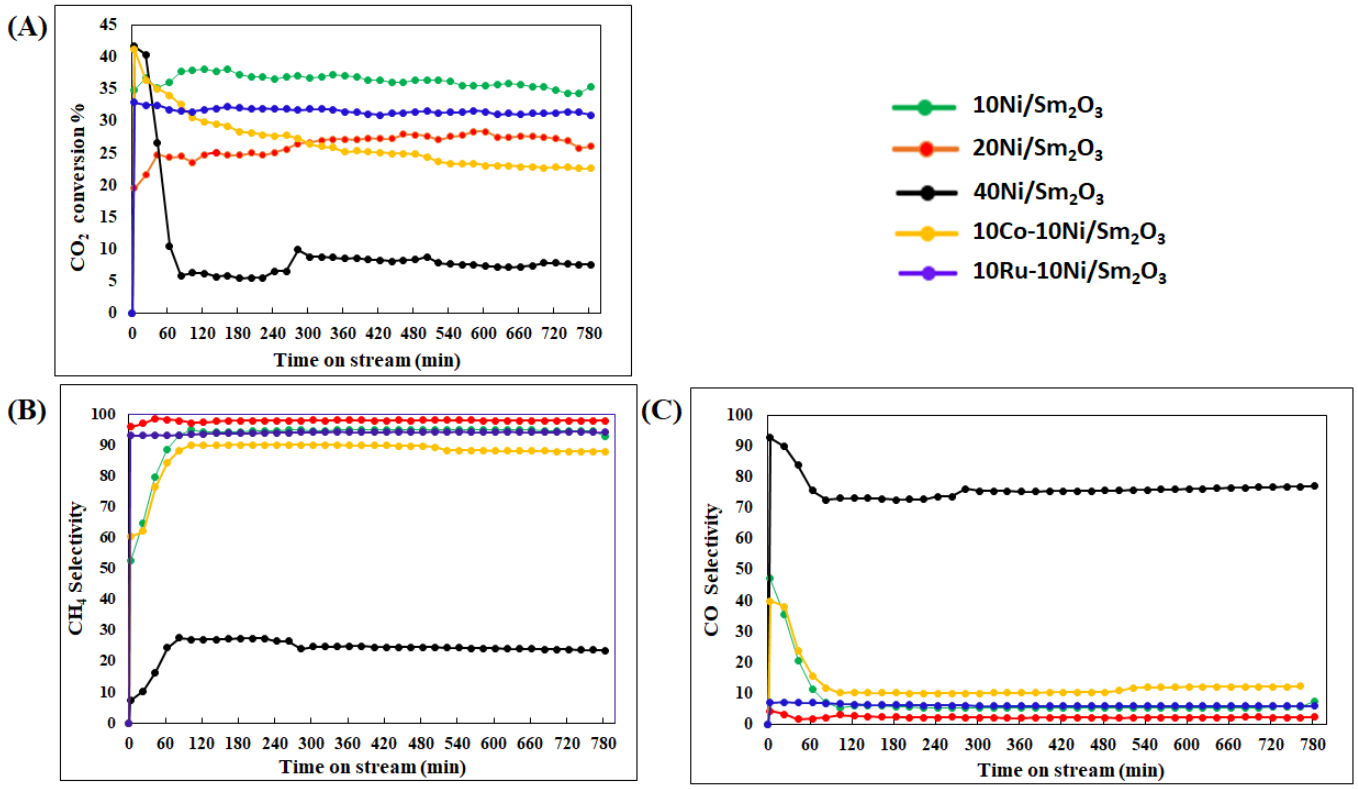


Figure 5. The catalytic activity vs. Time on stream of xNi/Sm_2O_3 (x = 10, 20, 40) and M-Ni/Sm_2O_3 (M = Co, Ru) catalysts at 350 °C reaction temperature over CO_2:H_2:Ar (1:4:5 volume ratio) feed gas: (**A**) CO_2 conversion vs. Time on stream (**B**) CH_4 selectivity vs. Time on stream (**C**) CO selectivity vs. Time on stream.

For 20.0 wt.% loading of Ni over Sm_2O_3, the NiO phase appeared in the X-ray diffraction pattern. Assembly of NiO particles might sign toward less dispersion of catalytic active species and it might provide limitation in higher activity toward CO_2 methanation. The surface area of the $20Ni/Sm_2O_3$ catalyst was four times that of $10Ni/Sm_2O_3$ and unidentate carbonate intensity in infrared spectra was also amplified. It had formate species and the highest number of reducible NiO species among the rest of the Ni-loaded Sm_2O_3 catalysts. However, the largely extendible surface and high amount of reducible NiO species over $20Ni/Sm_2O_3$ did not turn into higher CO_2 conversion, but it resulted in the highest CH_4 selectivity. The $20Ni/Sm_2O_3$ catalyst showed 24–26% CO_2 conversion, ~97–98% CH_4 selectivity, and 3–2% CO selectivity over 13 h of reaction. It indicated that a large number of reducible NiO species over large catalytic surfaces did not grant the higher CO_2 conversion by H_2. Hydrogen dissociation and its spillover concisely depend on the size of Ni particles. The higher NiO crystallinity over the $20Ni/Sm_2O_3$ catalyst than $10Ni/Sm_2O_3$ caused the formation of a relatively larger size of metallic Ni upon reduction, which limited H_2 dissociation and thereby CO_2 conversion. However, the relatively higher density of unidentate carbonate in the infrared spectrum of the $20Ni/Sm_2O_3$ catalyst indicated that limited H_2 dissociation, followed by CO_2 interaction over a largely extended surface, led to the formation of unidentate carbonate to methane via a stable formate path-

way. So, 20Ni/Sm_2O_3 conveyed highest ~98% CH_4 selectivity. The 10Ni/Sm_2O_3 catalyst needed some time for constant product selectivity, but the 20Ni/Sm_2O_3 catalyst gave constant product selectivity from the beginning. The surface mechanism over the samarium oxide-supported Ni system could be outlined at this stage. CO_2 was initially adsorbed as carbonate/bicarbonate species over the support of Sm_2O_3. The carbonate/bicarbonate species were hydrogenated to formate species. The formate species over Ni was stable and did not decompose into CO and H_2. Strong binding between Ni and the formate species guided the formate species to further hydrogenation to methane through methoxy intermediate (Route 5) [16]. The presence of a very small amount of CO over 20Ni/Sm_2O_3 indicated the initiation of further reaction of CH_4 with CO_2 (dry reforming of methane) or "CH_4 with H_2O" (stream reforming of methane) over the surface as metallic Ni also catalyzes CH_4 decomposition. For 40.0 wt.% impregnation of Ni over Sm_2O_3, the catalyst crystallinity was comparable to 10Ni/Sm_2O_3, but the surface area was decreased to the half and the amount of reducible NiO species over the catalyst surface was fallen suddenly. The shortage of reducible NiO species turned into a lower number of active sites (metallic Ni) after reduction. It caused just 8% CO_2 conversion. It appeared that, at such a high Ni loading, the formate species were majorly destabilized and decomposed into CO. Furthermore, the catalyst surface, bearing fewer active sites, was not so capable to push CO toward methanation. Overall, due to the destabilization of the formate-hydrogenation pathway over 40Ni/Sm_2O_3, two third of CO_2 was converted to CO and the remaining one third to CH_4 (75% CO selectivity and 25% CH_4 selectivity) during 180 min time-on-stream. To bring more focus to the reaction mechanism, Co-impregnation of Co-Ni and Ru-Ni over Sm_2O_3 support was carried out and was tested for CO_2 methanation reaction. When 10.0 wt.% Co and 10.0 wt.% Ni were co-impregnated over Sm_2O_3, the crystallinity of the catalyst was comparable to that of the 20Ni/Sm_2O_3, whereas it had the highest surface area and pore volume among all catalysts. Including reducible nickel oxide and cobalt oxide, the 10Co-10Ni/Sm_2O_3 catalyst had the highest intensity of reducible oxide over the catalyst surface. In addition, it had an adequate amount of formate species and the highest intensity of bicarbonate/carbonate species over the catalyst surface. Altogether, the 10Co-10Ni/Sm_2O_3 catalyst showed initially high CO_2 conversion (41%), which slowly and steadily dropped to 22% at the end of 13 h. Thus, diluting the active Ni sites by Co caused inferior catalytic activity in terms of CO_2 conversion. In EDX elemental analysis also, minimum Ni distribution over the surface was found in the case of the 10Co-10Ni/Sm_2O_3 catalyst (than the remaining catalysts). The product selectivity pattern over the 10Co-10Ni/Sm_2O_3 was very similar to the 10Ni/Sm_2O_3, namely, the 10Co-10Ni/Sm_2O_3 catalyst also needed some time for constant product selectivity. After 100 min, the 10Co-10Ni/Sm_2O_3 catalyst had attained 88–89% CH_4 selectivity and 12–11% CO selectivity. The relatively higher selectivity of CO over the 10Co-10Ni/Sm_2O_3 catalyst could be due to persuading reverse water–gas shift reaction over the cobalt-based catalyst [59]. When 10.0 wt.% Ru and 10.0 wt.% Ni were co-impregnated over Sm_2O_3, the cubic NiO phase was not found, but the tetragonal RuO_2 phase appeared. It had a good amount of reducible NiO and RuO_x species. It had an easier reducibility profile than other catalysts. The 10Ru-10Ni/Sm_2O_3 had five times less surface area and less surface adsorbed oxygen than the 10Co-10Ni/Sm_2O_3. Maximum surface distribution of Ni was confirmed over the 10Ru-10Ni/Sm_2O_3 catalyst by EDX elemental analysis (than rest catalyst). Among all catalyst systems, 10Ru-10Ni/Sm_2O_3 produced peaks for the carbonate species, but no peaks for the the formate species, indicating that the unstable formate species decomposed into CO. Further CO methanation might lead to methane formation over the 10Ru-10Ni/Sm_2O_3 catalyst. The previous literature also argued the mechanism of CO_2 methanation in the same line [6]. The 10Ru-10Ni/Sm_2O_3 catalyst had a higher catalytic activity (31–33% CO_2 conversion, 93–94% CH_4 selectivity, and ~6% CO selectivity constantly from the beginning to 13 h) than 10Co-10Ni/Sm_2O_3 due to the presence of more than one active site as Ni and Ru metals over the catalyst surface.

3. Materials and Methods

3.1. Materials

All chemicals were purchased and were used as received: Sm_2O_3 (99.9% AR from Loba Chemie, Mumbai, India), $Ni(NO_3)_2{\cdot}6H_2O$ (Acros Organics-Thermo Fisher Scientific, Geel, Belgium 99.9%), $Co(NO_3)_2{\cdot}6H_2O$ (Acros Organics-Thermo Fisher Scientific, 99.9%), and $RuCl_3{\cdot}xH_2O$ (Acros Organics-Thermo Fisher Scientific, 99.9%).

3.2. Catalyst Preparation

Samarium oxide-supported Ni, samarium oxide-supported Co-Ni, and samarium oxide-supported Ru-Ni catalysts were prepared by wet impregnation and co-impregnation methods. For supported Ni catalysts, an appropriate amount of $Ni(NO_3)_2{\cdot}6H_2O$ (equivalent to 10, 20, or 40 wt.% of Ni metal) was dissolved in water. For supported M-Ni (M = Co or Ru) bimetallic catalysts, an appropriate amount of metal precursor (equivalent to 10.0 wt.% Co or Ru) and Ni $(NO_3)_2{\cdot}6H_2O$ (equivalent to 10.0 wt.% Ni) were dissolved in water. In all, 3.0 g pre-calcined Sm_2O_3 (at 500 °C for five hours) was added as support to these aqueous solutions at 80 °C under slow stirring until complete evaporation for four hours. The slurries were kept overnight at 110 °C in the oven and were then calcined at 500 °C under air for three hours. The prepared catalysts were abbreviated as: $10Ni/Sm_2O_3$, $20Ni/Sm_2O_3$, $40Ni/Sm_2O_3$, $Co\text{-}Ni/Sm_2O_3$, and $Ru\text{-}Ni/Sm_2O_3$.

3.3. Catalysts Characterization

The surface area and porosity of catalyst samples were analyzed by NOVA 3200 apparatus (Quantachrome Corporation, Boynton Beach, FL, USA). Crystallinity and phase identification of the catalysts were studied by X-ray diffraction analysis (XRD) by using a Shimadzu XD-1 diffractometer (Kyoto, Japan). The presence of functional groups over the catalytic surface was studied by infrared spectroscopy by using a Nicolet Is-10 model, USA. The surface reducibility of the catalyst was studied under temperature programmed reduction under H_2-stream (H_2-TPR) by using a Chem BET 3000 (Quantachrome equipment, USA). The valance states of the elements and the binding energy of the bond electron were determined by X-ray photoelectron spectroscopy (XPS) by Themo Fisher Scientific, USA. The elemental mapping of catalyst samples was carried out by Energy Dispersive X-ray Spectroscopy instrument (Zeiss Smart EDX, Jena, Germany) equipped with a field-emission scanning electron microscope (FE-SEM; FEI Quanta FEG 250, Hilsboro, OR, USA). The detailed description of instrument and characterization procedure is given in the Supporting Information S6.

3.4. Catalyst Activity Test

Carbon dioxide methanation was carried out in a fixed-bed, tubular quartz silica reactor (length = 50 cm, Inner diameter = 13 mm), equipped with an electric furnace, having a programmable temperature controller. A total of 2.0 g of fresh catalyst was diluted with silicon carbide (to obtain a 5.0 cm bed height and 5 cm^3 volume of catalyst bed) and was packed in the middle of the reactor. The temperature of the catalyst bed was monitored by a K-type thermocouple, placed in the center of the catalyst bed. Prior to the reaction, the catalyst sample was reduced in situ with 30 mL/min H_2 flow at atmospheric pressure for two hours at 600 °C. After the reduction, the catalysts were cooled down, and CO_2:H_2:Ar (1:4:5 volume ratio) gas feed was passed through the activated catalyst at GHSV of 6000 $ccg^{-1}h^{-1}$. Afterwards, the temperature was increased to 350 °C and the methanation reaction was carried out for 13 h. Gaseous reaction products were analyzed online by a quantitative gas analysis system (HIDEN ANALYTICAL QGA, England, UK). The mol % of H_2, CO_2, CH_4, and CO was detected by gas analyzer by using a matrix equation to correct the overlapped detection values from the m/z of 28 (CO), 44 (CO_2), 2

(H_2), and 16 (CH_4). The carbon dioxide conversion (X_{CO_2}), methane selectivity (S_{CH_4}), and carbon monoxide selectivity (S_{CO}) were calculated using Equations (1)–(3) [21]:

$$X_{CO_2} = \frac{CO_{2,in} - CO_{2,out}}{CO_{2,in}} \times 100 \quad (1)$$

$$S_{CH_4} = \frac{CH_{4,out}}{CH_{4,out} + CO_{out}} \times 100 \quad (2)$$

$$S_{CO} = \frac{CO_{out}}{CH_{4,out} + CO_{out}} \times 100 \quad (3)$$

4. Conclusions

A Sm_2O_3-based Ni-supported catalyst was found excellent for CO_2 methanation at 350 °C reaction temperature. The 10Ni/Sm_2O_3 had the highest CO_2 conversion (35%) but needed some time (100 min) for constant high CH_4 selectivity (94–95%) over the 13 h reaction period. The 20Ni/Sm_2O_3 had larger NiO crystallite, which limited the H_2 dissociation and thereafter CO_2 conversion to 24–26%. However, the slower H_2 dissociation and interaction of CO_2 over a largely expanded surface showed the highest ~98% CH_4 selectivity from the beginning of the reaction. The formate species were stable at the Ni surface, as observed in the infrared spectra, which underwent further hydrogenation to methane. Despite the presence of the largest surface area and highest reducible metal oxide over the surface, 10Co-10Ni/Sm_2O_3 showed inferior catalytic performance because of diluting Ni sites by Co. On the other hand, diluting the Ni sites by Ru over Sm_2O_3 (10Ru-10Ni/Sm_2O_3 catalyst) caused again good catalytic activity. It had RuO_2 crystallite, very less surface parameters but easy reducibility. The absence of format species over the 10Ru-10Ni/Sm_2O_3 catalyst surface indicated an eight-electron reduction of intermediate CO into CH_4. In the mean of constant catalytic activity, the 10Ru-10Ni/Sm_2O_3 catalyst was found the best, as it showed 31–33% CO_2 conversion, and 93–94% CH_4 selectivity constantly from the beginning to the 13 h time-on-stream.

Supplementary Materials: The following supporting information can be downloaded at: https://www.mdpi.com/article/10.3390/catal13010113/s1, Figure S1. EDX elemental analysis of (A) 10Ni/Sm_2O_3 (B) 20Ni/Sm_2O_3 (C) 40Ni/Sm_2O_3 (D) 10Co-10Ni/Sm_2O_3 (E) 10Ni-10Ru/Sm_2O_3 catalysts; Figure S2. N_2 adsorption isotherm of Sm_2O_3 and 10Ni/Sm_2O_3 catalysts; Figure S3. Infrared transmittance spectra of Sm_2O_3 and 10Ni/Sm_2O_3 catalysts; Figure S4. Ru3d XPS spectrum of Ru-Ni/Sm_2O_3 catalyst. Figure S5. The methanation reaction over 10Ni/Sm_2O_3 at 3-different temperature for 1h at each 250 °C, 300 °C and 350 °C. Supporting Information S6. The detail description of instrument and characterization procedure.

Author Contributions: R.A.E.-S.: Project administration, investigation, methodology, conceptualization, formal analysis; A.S.A.-F.: supervision, data curation, methodology, validation, review, funding acquisition; K.A., W.U.K. and N.S.K.: formal analysis, writing—original draft; A.B. and A.A.I.: investigation, conceptualization, data curation; R.K. and A.A.M.A.: review, editing and supervision. All authors have read and agreed to the published version of the manuscript.

Funding: This research work was funded by Researchers Supporting Project number (RSP2023R368), King Saud University, Riyadh, Saudi Arabia.

Data Availability Statement: No data were used for the research described in the article.

Acknowledgments: The authors would like to extend their sincere appreciation to the Researchers Supporting Project number (RSP2023R368), King Saud University, Riyadh, Saudi Arabia.

Conflicts of Interest: The authors declare no conflict of interest.

References

1. Aziz, M.A.A.; Jalil, A.A.; Triwahyono, S.; Ahmad, A. CO_2 Methanation over Heterogeneous Catalysts: Recent Progress and Future Prospects. *Green Chem.* **2015**, *17*, 2647–2663. [CrossRef]
2. Navarro, J.C.; Centeno, M.A.; Laguna, O.H.; Odriozola, J.A. Policies and Motivations for the CO_2 Valorization through the Sabatier Reaction Using Structured Catalysts. A Review of the Most Recent Advances. *Catalysts* **2018**, *8*, 578. [CrossRef]
3. Saeidi, S.; Najari, S.; Fazlollahi, F.; Nikoo, M.K.; Sefidkon, F.; Klemeš, J.J.; Baxter, L.L. Mechanisms and Kinetics of CO_2 Hydrogenation to Value-Added Products: A Detailed Review on Current Status and Future Trends. *Renew. Sustain. Energy Rev.* **2017**, *80*, 1292–1311. [CrossRef]
4. 4Mandal, S.C.; Das, A.; Roy, D.; Das, S.; Nair, A.S.; Pathak, B. Developments of the Heterogeneous and Homogeneous CO_2 Hydrogenation to Value-Added C_{2+}-Based Hydrocarbons and Oxygenated Products. *Coord. Chem. Rev.* **2022**, *471*, 214737. [CrossRef]
5. Chiang, C.L.; Lin, K.S.; Chuang, H.W. Direct Synthesis of Formic Acid via CO_2 Hydrogenation over $Cu/ZnO/Al_2O_3$ Catalyst. *J. Clean. Prod.* **2018**, *172*, 1957–1977. [CrossRef]
6. Kwak, J.H.; Kovarik, L.; Szanyi, J. CO_2 Reduction on Supported Ru/Al_2O_3 Catalysts: Cluster Size Dependence of Product Selectivity. *ACS Catal.* **2013**, *3*, 2449–2455. [CrossRef]
7. Yu, Y.; Chan, Y.M.; Bian, Z.; Song, F.; Wang, J.; Zhong, Q.; Kawi, S. Enhanced Performance and Selectivity of CO_2 Methanation over G-C_3N_4 Assisted Synthesis of Ni–CeO_2 Catalyst: Kinetics and DRIFTS Studies. *Int. J. Hydrogen Energy* **2018**, *43*, 15191–15204. [CrossRef]
8. 8Hong, J.S.; Hwang, J.S.; Jun, K.W.; Sur, J.C.; Lee, K.W. Deactivation Study on a Coprecipitated Fe-Cu-K-Al Catalyst in CO_2 Hydrogenation. *Appl. Catal. A Gen.* **2001**, *218*, 53–59. [CrossRef]
9. Bansode, A.; Urakawa, A. Towards Full One-Pass Conversion of Carbon Dioxide to Methanol and Methanol-Derived Products. *J. Catal.* **2014**, *309*, 66–70. [CrossRef]
10. Wambach, J.; Baiker, A.; Wokaun, A. CO_2 Hydrogenation over Metal / Zirconia Catalysts CO CO Hydrogenation over Metal/Zirconia Catalysts. *Phys. Chem. Chem. Phys.* **1999**, *1*, 5071–5080. [CrossRef]
11. 1Ando, H.; Xu, Q.; Fujiwara, M.; Matsumura, Y.; Tanaka, M.; Souma, Y. Hydrocarbon Synthesis from CO_2 over Fe-Cu Catalysts. *Catal. Today* **1998**, *45*, 229–234. [CrossRef]
12. Kishan, G.; Lee, M.; Nam, S.; Choi, M.; Lee, K. The catalytic conversion of CO_2 to hydrocarbons over Fe–K supported on Al_2O_3–MgO mixed oxides. *Catal. Lett.* **1998**, *56*, 215–219.
13. Kim, J.; Lee, S.; Kang, M.; Lee, K.; Choi, M.; Kang, Y. Promotion of CO_2 hydrogenation to hydrocarbons in three-phase catalytic (Fe-Cu-K-Al) slurry reactors. *Korean J. Chem. Eng.* **2003**, *20*, 967–972.
14. Kim, J.S.; Lee, S.; Lee, S.B.; Choi, M.J.; Lee, K.W. Performance of Catalytic Reactors for the Hydrogenation of CO_2 to Hydrocarbons. *Catal. Today* **2006**, *115*, 228–234. [CrossRef]
15. Guo, M.; Lu, G. The Regulating Effects of Cobalt Addition on the Catalytic Properties of Silica-Supported Ni–Co Bimetallic Catalysts for CO_2 Methanation. *React. Kinet. Mech. Catal.* **2014**, *113*, 101–113. [CrossRef]
16. Deng, L.; Liu, X.; Wang, R.; Wang, C.; Zhou, G. Unsupported Ni-Co Alloy as Efficient Catalysts for CO_2 Methanation. *J. Alloys Compd.* **2022**, *918*, 165472. [CrossRef]
17. Owen, R.E.; O'Byrne, J.P.; Mattia, D.; Plucinski, P.; Pascu, S.I.; Jones, M.D. Cobalt Catalysts for the Conversion of CO_2 to Light Hydrocarbons at Atmospheric Pressure. *Chem. Commun.* **2013**, *49*, 11683–11685. [CrossRef]
18. Muroyama, H.; Tsuda, Y.; Asakoshi, T.; Masitah, H.; Okanishi, T.; Matsui, T.; Eguchi, K. Carbon Dioxide Methanation over Ni Catalysts Supported on Various Metal Oxides. *J. Catal.* **2016**, *343*, 178–184. [CrossRef]
19. Cai, M.; Wen, J.; Chu, W.; Cheng, X.; Li, Z. Methanation of Carbon Dioxide on Ni/ZrO_2-Al_2O_3 Catalysts: Effects of ZrO_2 Promoter and Preparation Method of Novel ZrO_2-Al_2O_3 Carrier. *J. Nat. Gas Chem.* **2011**, *20*, 318–324. [CrossRef]
20. Aziz, M.A.A.; Jalil, A.A.; Triwahyono, S.; Saad, M.W.A. CO_2 methanation over Ni-Promoted Mesostructured Silica Nanoparticles: Influence of Ni Loading and Water Vapor on Activity and Response Surface Methodology Studies. *Chem. Eng. J.* **2015**, *260*, 757–764. [CrossRef]
21. Zhao, K.; Wang, W.; Li, Z. Highly Efficient Ni/ZrO_2 Catalysts Prepared via Combustion Method for CO_2 Methanation. *J. CO2 Util.* **2016**, *16*, 236–244. [CrossRef]
22. Taherian, Z.; Yousefpour, M.; Tajally, M.; Khoshandam, B. A Comparative Study of ZrO_2, Y_2O_3 and Sm_2O_3 Promoted Ni/SBA-15 Catalysts for Evaluation of CO_2/Methane Reforming Performance. *Int. J. Hydrogen Energy* **2017**, *42*, 16408–16420. [CrossRef]
23. Vahid Shahed, G.; Taherian, Z.; Khataee, A.; Meshkani, F.; Orooji, Y. Samarium-Impregnated Nickel Catalysts over SBA-15 in Steam Reforming of CH_4 Process. *J. Ind. Eng. Chem.* **2020**, *86*, 73–80. [CrossRef]
24. Bazzi, S.; Schulz, E.; Mellah, M. Electrogenerated Sm(II)-Catalyzed CO_2 Activation for Carboxylation of Benzyl Halides. *Org. Lett.* **2019**, *21*, 10033–10037. [CrossRef]
25. Michel, C.R.; Martínez-Preciado, A.H.; Parra, R.; Aldao, C.M.; Ponce, M.A. Novel CO_2 and CO Gas Sensor Based on Nanostructured Sm_2O_3 Hollow Microspheres. *Sens. Actuators B Chem.* **2014**, *202*, 1220–1228. [CrossRef]
26. Yamasaki, M.; Komori, M.; Akiyama, E.; Habazaki, H.; Kawashima, A.; Asami, K.; Hashimoto, K. CO_2 Methanation Catalysts Prepared from Amorphous Ni-Zr-Sm and Ni-Zr-Misch Metal Alloy Precursors. *Mater. Sci. Eng. A* **1999**, *267*, 220–226. [CrossRef]
27. Ayub, N.A.; Bahruji, H.; Mahadi, A.H. Barium Promoted Ni/Sm_2O_3 Catalysts for Enhanced CO_2 Methanation. *RSC Adv.* **2021**, *11*, 31807–31816. [CrossRef]

28. El-Salamony, R.A.; El-Sharaky, S.A.; Al-Temtamy, S.A.; Al-Sabagh, A.M.; Killa, H.M. CO_2 Valorization into Synthetic Natural Gas (SNG) Using a Co–Ni Bimetallic Y2O3 Based Catalysts. *Int. J. Chem. React. Eng.* **2021**, *19*, 571–583. [CrossRef]
29. Suslick, K.S.; Skrabalak, S.E. *Handbook of Heterogeneous Catalysis*; Ertl, G., Knozinger, H., Weitkamp, J., Eds.; Wiley-VCH: Weinheim, Germany, 1997; Volume 4.
30. Yu, Q.; Yao, X.; Zhang, H.; Gao, F.; Dong, L. Effect of ZrO_2 Addition Method on the Activity of Al_2O_3-Supported CuO for NO Reduction with CO: Impregnation vs. Coprecipitation. *Appl. Catal. A Gen.* **2012**, *423–424*, 42–51. [CrossRef]
31. El-Salamony, R.A.; El-Sharaky, S.; El-Temtamy, S.; Al-Sabagh, A.; Killa, H. Effect of Ruthenium Promotor Ratio on Ni/Y_2O_3 Based Catalysts for CO_2 Methanation Reaction. *Egypt. J. Chem.* **2021**, *64*, 3–4. [CrossRef]
32. Sapkal, P.S.; Kuthe, A.M.; Kashyap, R.S.; Nayak, A.R.; Kuthe, S.A.; Kawle, A.P. Indirect Casting of Patient-Specific Tricalcium Phosphate Zirconia Scaffolds for Bone Tissue Regeneration Using Rapid Prototyping Methodology. *J. Porous Mater.* **2017**, *24*, 1013–1023. [CrossRef]
33. Vlasenko, N.V.; Kyriienko, P.I.; Valihura, K.V.; Kosmambetova, G.R.; Soloviev, S.O.; Strizhak, P.E. Yttria-Stabilized Zirconia as a High-Performance Catalyst for Ethanol to n-Butanol Guerbet Coupling. *ACS Omega* **2019**, *4*, 21469–21476. [CrossRef]
34. Salinas, D.; Escalona, N.; Pecchi, G.; Fierro, J.L.G. Lanthanum Oxide Behavior in La_2O_3-Al_2O_3 and La_2O_3-ZrO_2 Catalysts with Application in FAME Production. *Fuel* **2019**, *253*, 400–408. [CrossRef]
35. Lee, S.M.; Lee, Y.H.; Moon, D.H.; Ahn, J.Y.; Nguyen, D.D.; Chang, S.W.; Kim, S.S. Reaction Mechanism and Catalytic Impact of Ni/CeO_2- XCatalyst for Low-Temperature CO_2 Methanation. *Ind. Eng. Chem. Res.* **2019**, *58*, 8656–8662. [CrossRef]
36. Calatayud, M.; Collins, S.E.; Baltanás, M.A.; Bonivardi, A.L. Stability of Formate Species on β-Ga_2O_3. *Phys. Chem. Chem. Phys.* **2009**, *11*, 1397–1405. [CrossRef]
37. Xémard, M.; Goudy, V.; Braun, A.; Tricoire, M.; Cordier, M.; Ricard, L.; Castro, L.; Louyriac, E.; Kefalidis, C.E.; Clavaguéra, C.; et al. Reductive Disproportionation of CO_2 with Bulky Divalent Samarium Complexes. *Organometallics* **2017**, *36*, 4660–4668. [CrossRef]
38. Al-Fatesh, A.S.; Kumar, R.; Kasim, S.O.; Ibrahim, A.A.; Fakeeha, A.H.; Abasaeed, A.E.; Atia, H.; Armbruster, U.; Kreyenschulte, C.; Lund, H.; et al. Effect of Cerium Promoters on an MCM-41-Supported Nickel Catalyst in Dry Reforming of Methane. *Ind. Eng. Chem. Res.* **2022**, *61*, 164–174. [CrossRef]
39. Rahman, S.; Santra, C.; Kumar, R.; Bahadur, J.; Sultana, A.; Schweins, R.; Sen, D.; Maity, S.; Mazumdar, S.; Chowdhury, B. Highly Active Ga Promoted Co-HMS-$_\chi$ Catalyst towards Styrene Epoxidation Reaction Using Molecular O_2. *Appl. Catal. A Gen.* **2014**, *482*, 61–68. [CrossRef]
40. Hassan, S.; Kumar, R.; Tiwari, A.; Song, W.; van Haandel, L.; Pandey, J.K.; Hensen, E.; Chowdhury, B. Role of Oxygen Vacancy in Cobalt Doped Ceria Catalyst for Styrene Epoxidation Using Molecular Oxygen. *Mol. Catal.* **2018**, *451*, 238–246. [CrossRef]
41. Liu, N.; Du, R.J.; Li, W. Hydrogenation CO_2 to Formic Acid over Ru Supported on γ-Al_2O_3 Nanorods. *Adv. Mater. Res.* **2013**, *821–822*, 1330–1335. [CrossRef]
42. Löchel, B.P.; Strehblow, H.-H. Breakdown of Passivity of Nickel by Fluoride: II. Surface Analytical Studies. *J. Electrochem. Soc.* **1984**, *131*, 713–723. [CrossRef]
43. Mansour, A.N. Nickel Mg Kα XPS Spectra from the Physical Electronics Model 5400 Spectrometer. *Surf. Sci. Spectra* **1994**, *3*, 211–220. [CrossRef]
44. Mansour, A.N. Characterization of NiO by XPS. *Surf. Sci. Spectra* **1994**, *3*, 231–238. [CrossRef]
45. Khawaja, E.E.; Salim, M.A.; Khan, M.A.; Al-Adel, F.F.; Khattak, G.D.; Hussain, Z. XPS, Auger, Electrical and Optical Studies of Vanadium Phosphate Glasses Doped with Nickel Oxide. *J. Non-Cryst. Solids* **1989**, *110*, 33–43. [CrossRef]
46. Li, C.P.; Proctor, A.; Hercules, D.M. Curve fitting analysis of esca Ni 2p spectra of nickel-oxygen compounds and Ni/Al_2O_3 catalysts. *Appl. Spectrosc.* **1984**, *38*, 880–886. [CrossRef]
47. Klein, J.C.; Hercules, D.M. Surface Characterization of Model Urushibara Catalysts. *J. Catal.* **1983**, *82*, 424–441. [CrossRef]
48. Mandal, S.; Bando, K.K.; Santra, C.; Maity, S.; James, O.O.; Mehta, D.; Chowdhury, B. Sm-CeO_2 Supported Gold Nanoparticle Catalyst for Benzyl Alcohol Oxidation Using Molecular O_2. *Appl. Catal. A Gen.* **2013**, *452*, 94–104. [CrossRef]
49. Phenomena, R.; V, E.S.P.B.; Uwamino, Y.; Ishizuka, T.; Yamatera, H. X-ray photoelectron spectroscopy of rare-earth compounds. *J. Electron Spectrosc. Relat. Phenom.* **1984**, *34*, 67–78.
50. Reddy, B.M.; Chowdhury, B.; Smirniotis, P.G. XPS Study of the Dispersion of MoO_3 on TiO_2-ZrO_2, TiO_2-SiO_2, TiO_2-Al_2O_3, SiO_2-ZrO_2, and SiO_2-TiO_2-ZrO_2 Mixed Oxides. *Appl. Catal. A Gen.* **2001**, *211*, 19–30. [CrossRef]
51. Zhang, W.D.; Liu, B.S.; Zhan, Y.P.; Tian, Y.L. Syngas Production via CO_2 Reforming of Methane over Sm_2O_3-La_2O_3-Supported Ni Catalyst. *Ind. Eng. Chem. Res.* **2009**, *48*, 7498–7504. [CrossRef]
52. Lucentini, I.; Casanovas, A.; Llorca, J. Catalytic Ammonia Decomposition for Hydrogen Production on Ni, Ru and Ni[Sbnd]Ru Supported on CeO_2. *Int. J. Hydrogen Energy* **2019**, *44*, 12693–12707. [CrossRef]
53. Wang, Y.; Wang, J.; Xie, T.; Zhu, Q.; Zeng, D.; Li, R.; Zhang, X.; Liu, S. Ru Doping in Ni$(OH)_2$ to Accelerate Water Reduction Kinetics for Efficient Hydrogen Evolution Reaction. *Appl. Surf. Sci.* **2019**, *485*, 506–512. [CrossRef]
54. Italiano, C.; Llorca, J.; Pino, L.; Ferraro, M.; Antonucci, V.; Vita, A. CO and CO_2 Methanation over Ni Catalysts Supported on CeO_2, Al_2O_3 and Y_2O_3 Oxides. *Appl. Catal. B Environ.* **2020**, *264*, 118494. [CrossRef]
55. Yan, Y.; Dai, Y.; Yang, Y.; Lapkin, A.A. Improved Stability of Y_2O_3 Supported Ni Catalysts for CO_2 Methanation by Precursor-Determined Metal-Support Interaction. *Appl. Catal. B Environ.* **2018**, *237*, 504–512. [CrossRef]
56. Falbo, L.; Visconti, C.G.; Lietti, L.; Szanyi, J. The Effect of CO on CO_2 Methanation over Ru/Al_2O_3 Catalysts: A Combined Steady-State Reactivity and Transient DRIFT Spectroscopy Study. *Appl. Catal. B Environ.* **2019**, *256*, 117791. [CrossRef]

57. Yin, G.; Yuan, X.; Du, X.; Zhao, W.; Bi, Q.; Huang, F. Efficient Reduction of CO_2 to CO Using Cobalt–Cobalt Oxide Core–Shell Catalysts. *Chem.-A Eur. J.* **2018**, *24*, 2157–2163. [CrossRef]
58. Guilera, J.; Del Valle, J.; Alarcón, A.; Díaz, J.A.; Andreu, T. Metal-Oxide Promoted Ni/Al_2O_3 as CO_2 Methanation Micro-Size Catalysts. *J. CO2 Util.* **2019**, *30*, 11–17. [CrossRef]
59. Kumar, R.; Shah, S.; Bahadur, J.; Melnichenko, Y.B.; Sen, D.; Mazumder, S.; Vinod, C.P.; Chowdhury, B. Highly Stable In-SBA-15 Catalyst for Vapor Phase Beckmann Rearrangement Reaction. *Microporous Mesoporous Mater.* **2016**, *234*, 293–302. [CrossRef]

Disclaimer/Publisher's Note: The statements, opinions and data contained in all publications are solely those of the individual author(s) and contributor(s) and not of MDPI and/or the editor(s). MDPI and/or the editor(s) disclaim responsibility for any injury to people or property resulting from any ideas, methods, instructions or products referred to in the content.